Intramolecular Hydrogen Bonding in the $S_1(\pi\pi^*)$ Excited State of Anthranilic Acid and Salicylic Acid: TDDFT Calculation of Excited-State Geometries and Infrared Spectra

Andrzej L. Sobolewski*,† and Wolfgang Domcke‡

Institute of Physics, Polish Academy of Sciences, PL-02668 Warsaw, Poland, and Department of Chemistry, Technical University of Munich, D-85747 Garching, Germany

Received: August 9, 2004; In Final Form: September 27, 2004

The equilibrium geometries and vibrational spectra of anthranilic acid (AA) and salicylic acid (SA) in the $S_1(\pi\pi^*)$ excited state have been determined with time-dependent density functional theory (TDDFT). A single minimum of the excited-state potential-energy surface, rather than separate amino/imino (enol/keto) minima, is found for AA and SA. A significant strengthening of the intramolecular hydrogen bond upon electronic excitation is predicted for both systems. The excited-state minimum corresponds to a shortening of the intramolecular hydrogen bond by 0.226 Å (0.322 Å) in AA (SA). The calculated 0−0 excitation energies are within 0.1 eV of the experimental values. An exceptionally large red shift of 1400 cm^{-1} and a strong mixing with H-chelate ring bending and stretching motions is predicted for the phenolic OH stretching vibration in the S_1 state of salicylic acid. In anthranilic acid, a red shift of 500 cm^{-1} is obtained for the H-bonded amino NH stretching vibration, in excellent agreement with a recent UV−IR double-resonance experiment [Southern, D. A.; Levy, D. H.; Florio, G. M.; Longarte, A.; Zwier, T. S. *J. Phys. Chem. A* **2003**, *107*, 4032]. The results suggest that the TDDFT method with the B3LYP functional is a viable method for the calculation of excited-state potential-energy surfaces of intramolecularly hydrogen-bonded aromatic systems.

1. Introduction

Since the early work of Weller on methyl salicylate,[1] salicylic acid (SA, see Scheme 1) has served as a model compound for the experimental and theoretical investigation of the excited-state intramolecular hydrogen-transfer (ESIHT) reaction (see, for example, refs 2−9). The observation of a strongly Stokes-shifted visible fluorescence band has been interpreted as the signature of an exothermic intramolecular proton-transfer process in the $S_1(\pi\pi^*)$ excited state of SA. Weller assumed that the excited-state product is a zwitterion, which led to the concept of intramolecular proton transfer. Meanwhile, calculations have revealed that there is no significant change of the electric dipole moment associated with this process, that is, a hydrogen atom is moving rather than a proton.[7−9] Therefore, the acronym ESIHT will be used throughout this paper, rather than the original acronym ESIPT (excited-state intramolecular proton transfer).

Investigations of dispersed fluorescence spectra of SA in the gas phase and in supersonic jets have led to the proposition that only a rather moderate elongation of the phenolic OH bond length takes place in the $S_1(\pi\pi^*)$ excited state, rather than a full enol-to-keto hydrogen transfer.[3−5] This interpretation of the fluorescence spectra is supported by calculations of the energy profile along the hydrogen-transfer reaction path, which was found to exhibit a single minimum corresponding to a moderate extension (by about 0.17 Å) of the phenolic OH bond length.[7,8]

As is well-known, the vibrational frequencies of the stretching vibrations of OH or NH groups involved in hydrogen bonding provide a clear-cut signature of the strength of these hydrogen bonds.[10,11] Yahagi et al. recently have reported the infrared (IR) spectra of SA in the S_0 and $S_1(\pi\pi^*)$ states in the frequency range of OH stretching vibrations, employing UV−IR double-resonance techniques.[6] The phenolic OH stretching vibration of SA was not observed in the S_1 state in the range 2400−3600 cm^{-1}. Yahagi et al. estimated that an OH bond-length extension of 0.17 Å, as predicted by the calculations,[7] could shift the OH stretching frequency in the S_1 state below 2400 cm^{-1} and thus out of the detection range.[6]

SCHEME 1

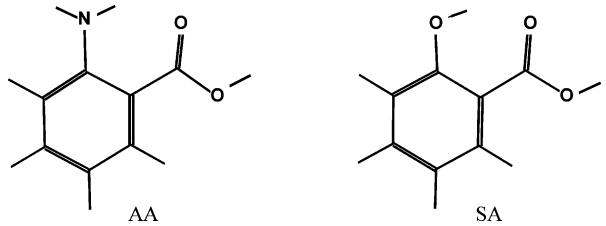

Very recently, Levy, Zwier, and collaborators have recorded similar UV−IR double-resonance spectra for anthranilic acid (AA), Scheme 1.[12] The replacement of the phenolic OH group by the amino group results in a weaker intramolecular hydrogen bond in the S_0 state. A red shift of 500 cm^{-1} of the NH stretching frequency in S_1 relative to S_0 has been observed,[12] which indicates a substantial strengthening of the intramolecular hydrogen bond in the excited state.

Ab initio calculations of vibrational frequencies and IR intensities in the $S_1(\pi\pi^*)$ state of SA and AA clearly are highly desirable for the assignment of the spectra. While such calculations are a routine exercise for the S_0 state (using MP2 or DFT methods), meaningful frequency calculations were not possible until recently for the excited state of SA and related compounds. As has been discussed in detail in refs 7, 9, and 14, both the CIS (single-excitation configuration interaction) and CASSCF (complete-active-space self-consistent-field) methods, which can routinely be used for excited-state geometry optimizations and

† Polish Academy of Sciences.
‡ Technical University of Munich.

10.1021/jp046428s CCC: $27.50
Published on Web 11/11/2004

TABLE 1: Harmonic Vibrational Frequencies (in cm^{-1}), IR Intensities (in km/mol), and Assignments of the Character of the Normal Modes of Anthranilic Acid in the S_0 and $S_1(\pi\pi^*)$ Electronic States[a]

S_0			S_1(H)			S_1(D)		
freq	intens	assignment	freq	intens	assignment	freq	intens	assignment
i121 (88)[b]		NH_2 oop	105	1.8	carboxy twist/NH_2 oop	105	1.8	carboxy twist/NH_2 oop
97	5.7	carboxy twist	142	0.3	inter-ring twist	142	0.3	inter-ring twist
174	40.0	NH oop	246	10.9	inter-ring oop	244	11.0	inter-ring oop
241	8.1	inter-ring oop	268	4.1	carboxy bend	266	5.1	carboxy bend
255	1.1	carboxy bend	344	21.9	ring/NH oop	344	21.9	ring/NH oop
369	8.8	CN bend	373	42.7	CN bend	360	37.8	CN bend
419	1.5	H-ring defor	425	5.9	H-ring defor	419	9.1	H-ring defor
431	4.3	ring oop	429	10.2	NH/OH oop	429	10.0	NH/OH oop
510	3.9	inter-ring bend	490	4.6	ring oop	487	2.6	ring oop
542	9.0	ring oop	510	4.3	inter-ring defor	505	3.9	inter-ring defor
568	1.1	ring defor	530	106.7	OH twist	530	109.0	OH twist
589	80.9	OH twist	556	12.8	ring defor	552	13.7	ring defor
625	9.1	NH_2 twist	609	44.3	ring/OCO oop	604	37.1	ND/OH oop
650	50.4	ring defor/OCO bend	621	30.9	ring/OCO bend	616	57.1	ND/OH oop
723	38.0	ring/OCO oop	673	25.0	CH oop	618	43.3	CH/ND oop
751	15.2	ring/COH bend	719	8.8	CH oop	680	11.1	CH oop
768	34.2	CH oop	733	9.8	ring/OCO bend	731	22.1	CH oop
811	5.7	CH/COO oop	817	5.4	CH/NH oop	733	11.6	ring/OCO bend
864	4.3	CH oop	825	5.1	CH oop	822	0.7	CH oop
865	5.8	ring defor	848	38.4	ring defor	826	9.7	CH oop
973	0.1	CH oop	869	56.3	NH oop	840	32.7	ring defor
993	0.1	CH oop	939	1.1	CH oop	939	0.9	CH oop
1041	4.3	CC str/NH_2 bend	1023	48.5	CC str	973	22.3	NHD bend
1071	12.4	CC str	1049	36.5	CC str	1032	67.7	CC str
1100	94.0	NH_2 bend/C−O str	1078	152.8	CC/C−O str/NH_2 bend	1055	174.3	CC str
1167	70.0	CH bend	1140	54.4	NH_2/CH bend	1103	6.2	CH bend
1174	42.9	CH bend	1156	20.6	CH bend	1156	20.2	CH bend
1206	276.4	OH bend	1221	219.6	OH bend	1218	243.0	OH bend
1302	2.1	CH bend	1282	18.3	CC/CN str	1248	94.0	CN str/HND bend
1346	30.9	CN str/CH bend	1304	52.2	CN/CH bend	1282	23.2	CH bend
1377	77.6	CC/C−O str	1360	163.8	C−O str	1352	143.7	C−O str/
1411	56.1	CC str/CH bend	1385	58.9	CC str/CH bend	1380	74.3	CC str/CH bend
1487	3.3	CH/NH bend	1446	14.6	CH bend	1391	3.3	CC str/ND bend
1511	25.0	CC str/CH bend	1458	64.9	CC str/CH bend	1443	9.5	CH bend
1584	145.3	CN str/HNH bend	1509	305.2	CC str/NH bend	1458	61.0	CC str/CH bend
1618	150.8	CC str/NH bend	1546	92.9	HNH bend	1518	274.0	CC str/CH bend
1668	112.5	CC str	1569	3.9	CC str/CH bend	1568	6.2	CC str/CH bend
1758	349.6	C═O str	1705	132.4	C═O str/NH bend	1693	175.9	C═O str
3160	9.1	CH str	3019	457.1	NH_{bond} str	2240	251.9	ND str
3179	18.0	CH str	3173	13.3	CH str	3173	12.3	CH str
3197	11.5	CH str	3183	23.3	CH str	3183	21.9	CH str
3220	4.5	CH str	3217	10.3	CH str	3217	10.8	CH str
3514	121.9	NH_{sym} str	3230	5.3	CH str	3230	4.8	CH str
3700	74.5	NH_{asym} str	3624	57.2	NH_{free} str	3619	47.0	NH str
3720	85.9	OH str	3742	109.4	OH str	3742	111.0	OH str

[a] The data for the S_1 state of singly deuterated anthranilic acid are given for comparison. The DFT(TDDFT) method has been employed for the $S_0(S_1)$ state. No scaling factors have been applied. [b] Calculated at C_1 symmetry.

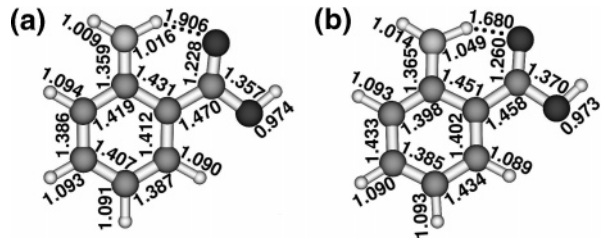

Figure 1. Equilibrium geometry of anthranilic acid in the electronic ground state (a) and in the $S_1(\pi\pi^*)$ state (b), optimized at the DFT and TDDFT levels, respectively. Bond lengths are given in Å.

harmonic frequency calculations, yield qualitatively incorrect results for SA, predicting separate enol and keto-type minima, rather than a single minimum, as predicted by the more accurate CASPT2 (second-order perturbation theory on the CASSCF reference) method.

Exploratory calculations with time-dependent density functional theory (TDDFT)[15,16] for the prototypical molecules SA and *o*-hydroxybenzaldehyde have shown that TDDFT yields reaction-path potential-energy profiles which are essentially parallel to those obtained with the CASPT2 method.[9] This finding suggests that TDDFT may be a potentially useful method for the calculation of the excited-state vibrational spectra of ESIHT systems. The recent implementation of TDDFT analytic gradients in several quantum chemistry packages permits efficient excited-state geometry optimizations and vibrational frequency calculations at the TDDFT level.[17−19]

In the present work, we have employed the TDDFT method for the calculation of excited-state minimum geometries, vibrational frequencies, and IR intensities of SA and AA. Only rotamer I (see refs 4 and 12) of SA and AA is considered, because only this rotamer possesses a strong intramolecular hydrogen bond.

2. Computational Details

All calculations were performed with Becke's three-parameter hybrid functional (B3LYP).[20] Dunning's correlation consistent

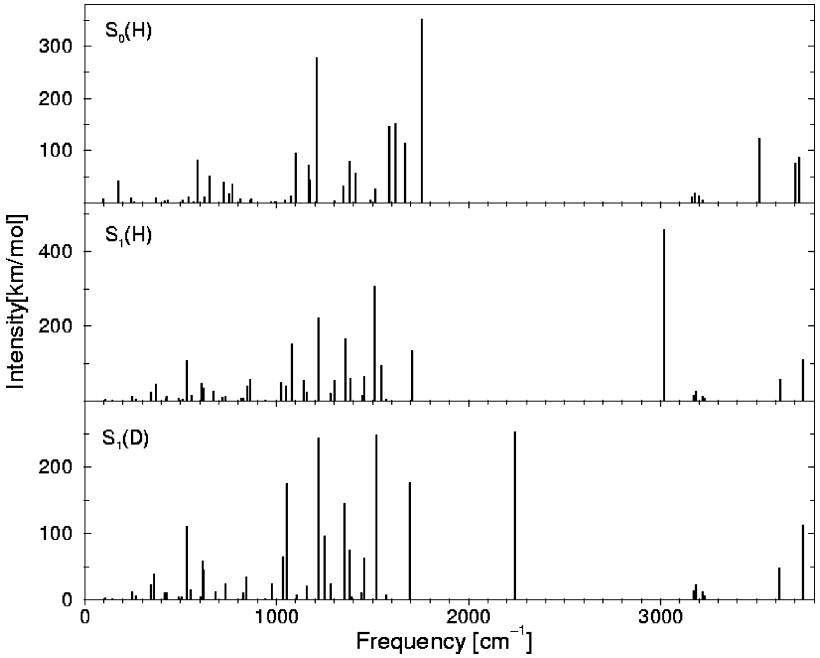

Figure 2. Infrared absorption spectrum of anthranilic acid in the electronic ground state (upper panel) and in the $S_1(\pi\pi^*)$ state (middle panel). The IR spectrum of the S_1 state of singly deuterated anthranilic acid is shown in the lower panel. The spectra have been calculated in the harmonic approximation with the DFT (S_0) and TDDFT (S_1) methods.

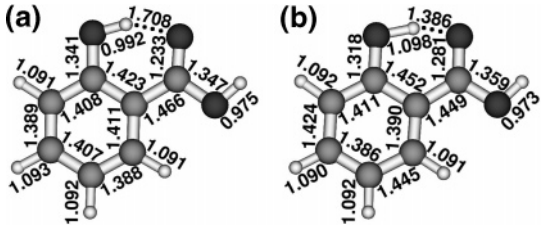

Figure 3. Equilibrium geometry of salicylic acid in the electronic ground state (a) and in the $S_1(\pi\pi^*)$ state (b), optimized at the DFT and TDDFT levels, respectively. Bond lengths are given in Å.

basis set of double-ζ quality with polarization functions on all atoms (cc-pVDZ)[21] was used in the calculations. We prefer this basis set over the more popular Pople-type basis set because it is better designed to treat electronically excited states. The excited-state geometry optimizations were performed at the TDDFT level, while the DFT method was used for the ground-state optimizations. Harmonic vibrational frequencies in the ground state and the excited state were determined by diagonalization of the Hessian. The excited-state Hessian was obtained by numerical differentiation of the analytical gradients. All calculations were carried out with the TURBOMOLE program suite[22] with default settings for the convergence thresholds for optimization and the nuclear displacements used in the numerical differentiation of the gradient. The IR intensities were determined from the gradients of the dipole moment.

3. Anthranilic Acid

3.1. Ground-State Geometry and IR Spectrum. The ground-state equilibrium geometry of anthranilic acid has been optimized at the DFT level with C_s symmetry constraint. The resulting structure, the amino tautomer, is shown in Figure 1a. The proton-transferred (imino) tautomer does not seem to exist as a stationary point of the ground-state potential-energy surface; all attempts to optimize the imino structure lead to the amino tautomer.

The frequency calculation reveals one imaginary frequency (ω = i121 cm^{-1}) of the C_s-constrained stationary point. The corresponding normal coordinate leads to a pyramidization of the amino group. Relaxation of the C_s symmetry constraint results in a stable minimum structure of C_1 symmetry with a slightly pyramidized amino group (CCNH dihedral angles of 8.7° and 12.8° for the H-bonded and free NH bond, respectively). At this level of theory, the nonplanar equilibrium structure is more stable than the planar structure by 0.25 kcal/mol (87.5 cm^{-1}). The amino wagging frequency of the C_1 structure is 88 cm^{-1}. AA thus is quasiplanar in the S_0 state. Very similar results have been obtained by Southern et al. with the 6-31G(d, p) basis set.[12] For better comparison with the vibrational spectrum of the planar S_1 state and for easier assignment of the normal modes, we report in Table 1 the vibrational frequencies and IR intensities of the C_s-constrained S_0 equilibrium structure.

The ground-state IR spectrum of anthranilic acid in the hydride stretch region has been measured and assigned by Southern et al. by comparison with scaled (scaling factor 0.9528) DFT/B3LYP vibrational frequencies. We refer to this paper for a more detailed discussion of the ground-state IR spectrum.

3.2. Excitation Energy and Excited-State Geometry. The calculated vertical excitation energy of the $S_1(\pi\pi^*)$ state of AA is 3.92 eV. The TDDFT geometry optimization of the S_1 state yields, as in the S_0 state, the amino tautomer as the single stable structure. In contrast to the ground-state equilibrium geometry, the amino group is planar in the excited state, i.e., the S_1 equilibrium structure has C_s symmetry. This structure is shown in Figure 1b.

Electronic excitation to the $S_1(\pi\pi^*)$ state results in moderate changes of geometry of the aromatic ring. The most pronounced effect is the interchange of the single/double bond character of bonds, which is reflected by the bond lengths. The electronic excitation substantially increases the strength of the intramolecular hydrogen bond, which is indicated by the decrease of the H-bond length from 1.906 Å in the S_0 state to 1.680 Å in the S_1 state, see Figure 1. The length of the hydrogen-bonded NH bond increases moderately (by 0.033 Å) due to electronic

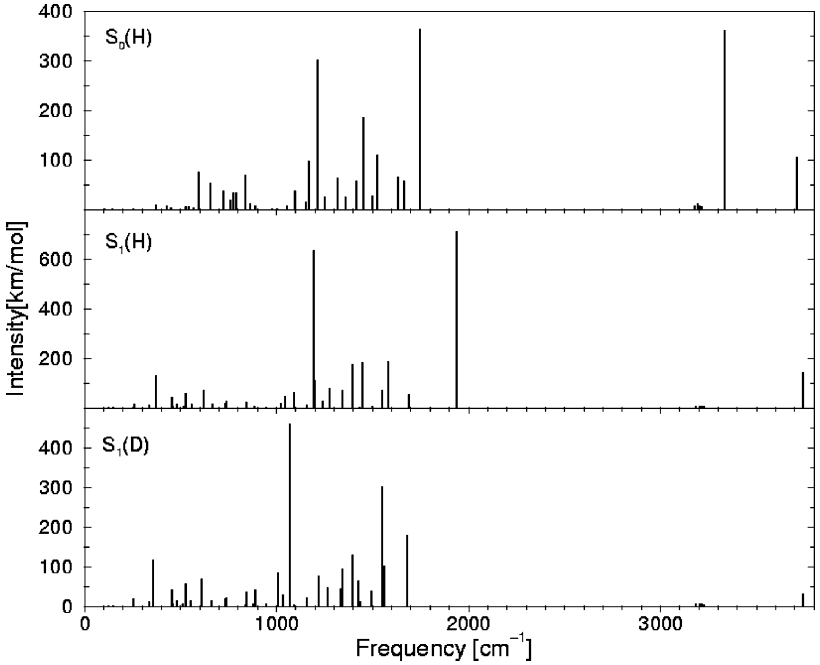

Figure 4. Infrared absorption spectrum of salicylic acid in the electronic ground state (upper panel) and in the $S_1(\pi\pi^*)$ state (middle panel). The IR spectrum of the S_1 state of singly deuterated salicylic acid is shown in the lower panel. The spectra have been calculated in the harmonic approximation with the DFT (S_0) and TDDFT (S_1) methods.

excitation. Clearly, no ESIHT reaction takes place in the $S_1(\pi\pi^*)$ state of AA.

The adiabatic electronic excitation energy, calculated as the difference between the DFT energy of the ground state and the TDDFT energy of the $S_1(\pi\pi^*)$ state at their respective equilibrium geometries, is 3.67 eV (29 600 cm^{-1}). Correction for the zero-point vibrational energy, using the harmonic vibrational frequencies listed in Table 1, reduces this value to 3.46 eV (27 900 cm^{-1}). This energy is 0.08 eV (680 cm^{-1}) lower than the experimental value of 28 580 cm^{-1}.[12] The agreement between theory and experiment is excellent in this case.

3.3. Excited-State IR Spectrum. The calculated vibrational frequencies of the $S_1(\pi\pi^*)$ state and their assignments are given in Table 1, together with the frequencies of singly deuterated AA. The IR spectra (fundamental vibrational frequencies and intensities), calculated in the harmonic approximation, of AA and singly deuterated AA (AA(D)) are shown in Figure 2 in comparison with the calculated ground-state IR spectrum of SA.

Despite the relatively small changes in the equilibrium geometry upon electronic excitation, the IR spectrum of the S_1 state differs substantially from that of the S_0 state, see Figure 2 and Table 1. The C═O stretching band (1758 cm^{-1}), which dominates the IR spectrum of the ground state, is downshifted to 1705 cm^{-1}, and loses intensity. This effect is in qualitative agreement with a recent experiment[13] that shows a somewhat larger reduction of the frequency (78 cm^{-1}) and a similar loss of intensity. The most pronounced changes occur for the H-bonded stretching line. This line is shifted from 3514 cm^{-1} in the S_0 state to 3019 cm^{-1} in the S_1 state and thus below the CH stretching lines. Its intensity increases substantially (see Figure 2). The calculated frequency shift is in excellent agreement with the measured shift of 500 cm^{-1}.[12] The experimental IR−UV double resonance spectrum, on the other hand, indicates a significant reduction of the intensity of this line compared with the ground-state OH stretch line. The origin of this apparent discrepancy between computation and experiment must remain open at present. We mention that it is a general observation in intramolecular hydrogen-bonded molecules as well as hydrogen-bonded clusters that the IR bands of OH or NH bonds involved in strong hydrogen bonding experience a pronounced red shift, broadening, and enhancement in intensity.[10,11] The theoretically predicted intensity enhancement of the OH stretch line in the S_1 state is in accord with this general experience. The present results fully support the assignments of the measured excited-state IR spectrum in ref 12.

Deuteration leads to the expected reduction of the ND frequency by a factor of $\sqrt{2}$ (from 3514 to 2240 cm^{-1}). Both in AA(H) and in AA(D), the NH/ND line is located in a window region of the IR spectrum (see Figure 2) and thus relatively easily detectable.

4. Salicylic Acid

4.1. Ground-State Geometry and IR Spectrum. The ground-state geometry of SA obtained with the DFT/B3LYP method is shown in Figure 3a. The structure is planar at the MP2[7] and DFT/B3LYP[6] levels. The data are included in Figure 3a for consistent comparison with the S_1 equilibrium geometry shown in Figure 3b. The OH bond length of the phenolic OH group is 0.992 Å, and the length of the H···O hydrogen bond is calculated as 1.708 Å, reflecting a fairly strong intramolecular hydrogen bond.

The calculated S_0 IR spectrum is shown in the upper panel of Figure 4. It is dominated by three intense lines at 3330 (H-bonded OH stretch), 1750 (CO stretch), and 1210 cm^{-1} (H-chelate ring deformation). The S_0 IR spectrum in the OH stretch region has been recorded and assigned by Yahagi et al.[6] The present results fully agree with their assignments.

4.2. Excitation Energy and Excited-State Geometry. The S_1 vertical excitation energy of SA calculated at the TDDFT level is 4.20 eV, which may be compared with the CASPT2 result of 3.92 eV.[7] The adiabatic excitation energy, calculated as the difference of the TDDFT energy of S_1 and the DFT energy of S_0 at their respective minima, is 3.92 eV (31 600 cm^{-1}). Inclusion of zero-point vibrational energies, using the harmonic vibrational frequencies of Table 2, yields a value of

TABLE 2: Harmonic Vibrational Frequencies (in cm^{-1}), IR Intensities (in km/mol), and Assignments of the Character of the Normal Modes of Salicylic Acid in the S_0 and in $S_1(\pi\pi^*)$ Electronic States[a]

S_0			S_1(H)			S_1(D)		
freq	intens	assignment	freq	intens	assignment	freq	intens	assignment
102	0.2	carboxy twist	124	0.	carboxy twist	124	0.5	carboxy twist
145	0.6	inter-ring twist	149	0.1	inter-ring twist	149	0.1	inter-ring twist
250	0.8	inter-ring oop	251	1.9	inter-ring oop	250	4.7	inter-ring oop
250	1.0	carboxy bend	256	14.1	inter-ring bend	253	17.0	inter-ring bend
371	9.3	CO_{hydr} bend	335	7.3	ring oop	334	10.7	ring oop
429	6.8	ring oop	372	127.0	H-ring deform	354	116.0	H-ring defor
446	2.9	H-ring defor	451	41.2	$OH_{carboxy}$ twist	451	40.9	$OH_{carboxy}$ twist
526	3.9	inter-ring bend	458	3.1	H-ring deform	456	5.4	H-ring deform
543	3.7	ring oop	478	13.8	ring oop	478	13.7	ring oop
568	2.5	ring defor	513	5.1	ring deform	508	5.0	inter-ring defor
595	74.8	$OH_{carboxy}$ twist	527	56.8	$OH_{carboxy}$ twist	526	56.4	$OH_{carboxy}$ twist
652	52.2	ring defor/OCO bend	557	13.5	ring deform	554	13.8	ring defor
722	36.9	ring oop	620	68.7	H-ring deform	610	68.6	H-ring deform
758	18.0	ring defor/OCO bend	665	11.3	CH oop	661	13.0	CH oop
774	32.4	CH oop	734	17.1	ring deform/OCO bend	732	16.7	CH oop
791	32.8	COO/CH oop	740	24.9	CH oop	736	19.6	CH oop
836	68.2	OH_{hydr} twist	843	21.0	CH oop	838	2.7	CH oop
862	10.7	ring defor	843	19.5	CH oop	841	36.1	ring defor
885	6.5	CH oop	881	6.0	CH oop	876	6.6	OD/CH oop
976	0.4	CH oop	945	1.9	CH oop	887	40.4	OD/CH oop
1004	0.4	CH oop	1021	16.3	CC str	946	6.2	CH oop
1052	7.3	CC str	1043	45.0	CC str	1006	83.0	CC str/H disloc
1096	35.9	CC/C−$O_{carboxy}$ str	1090	59.7	CC str	1030	27.5	CC str
1153	14.4	CH bend	1156	8.7	CH bend	1067	457.3	CC/OD str
1169	97.1	CH bend	1194	634.2	OH bend	1090	2.4	CH bend
1211	300.0	$OH_{carboxy}$ bend	1199	109.5	OH_{hydr} twist	1159	20.7	CH bend
1251	24.7	CH/OHbend	1239	23.2	OH/CH bend	1220	74.3	OH bend
1319	62.0	CC/CO_{hydr} str	1277	78.6	CH bend	1263	46.0	CH bend
1360	23.7	CC str/OH bend	1340	67.1	CO_{hydr} str/CH bend	1331	43.3	CH//OD bend
1415	57.2	CC/$CO_{carboxy}$ str	1396	173.6	CC str/CH bend	1345	92.7	OD deform/CH bend
1452	184.6	CC str/OH bend	1429	2.4	CH bend	1394	126.8	CC str/CH bend
1497	26.8	CC/$CO_{carboxy}$ str	1448	181.5	CC/CO_{hydr} str	1423	62.6	CC/CO str
1522	108.2	CH/OH_{hydr} bend	1496	2.8	CC str/CH bend	1438	9.2	CH bend
1632	65.3	CC str/OH_{hydr} bend	1551	69.5	CC str/H disloc	1494	38.0	CC/C−O str/CH bend
1665	56.5	CC str	1580	184.6	CC str/H disloc	1551	301.1	CC/OD str
1746	362.2	C═O str	1686	52.3	C═O str/OH bend	1562	101.0	CC str/CH bend
3176	6.0	CH str	1937	709.6	H detach	1678	178.8	C═O str/OH bend
3195	9.5	CH str	3185	6.3	CH str	3185	6.1	CH str
3206	6.0	CH str	3206	6.6	CH str	3206	6.6	CH str
3214	4.5	CH str	3213	6.6	CH str	3213	6.3	CH str
3332	359.6	OH_{hydr} str	3225	3.2	CH str	3225	3.3	CH str
3709	105.9	$OH_{carboxy}$ str	3742	141.4	$OH_{carboxy}$ str	3742	31.1	OH str

[a] The data for the S_1 state of singly deuterated salicylic acid are included for comparison. The DFT(TDDFT) method has been employed for the $S_0(S_1)$ state. No scaling factors have been applied.

3.76 eV (30 400 cm^{-1}). This value is 0.07 eV (580 cm^{-1}) higher than the experimental value of 29 820 cm^{-1}.[4] It is seen that TDDFT performs surprisingly well for the $S_1(\pi\pi^*)$ excitation energies of this intramolecularly hydrogen-bonded aromatic system.

Inspection of Figure 3 reveals that the most drastic geometry change upon $S_0 \rightarrow S_1$ excitation is the shortening of the intramolecular hydrogen bond, from 1.708 to 1.386 Å, a bond-length shortening of 0.322 Å. The length of the phenolic OH bond, on the other hand, increases by 0.106 Å. Both bond-length changes indicate a very significant strengthening of the intramolecular hydrogen bond in the S_1 state of SA. The H atom remains bonded, however, to the phenolic oxygen. No hydrogen transfer takes place in the S_1 state of SA, in agreement with previous predictions and assignments.[3−5,7−9] Although the S_1 equilibrium structure is nominally enolic (see, however, the comment 23), the H-chelate ring is more symmetric than in the ground state, indicating a significant conjugation of the bonds.

4.3. Excited-State IR Spectrum. The calculated IR spectra of SA and singly deuterated SA (SA(D)) in the S_1 state are shown in Figure 4 in comparison with the ground-state IR spectrum of SA. The vibrational frequencies and intensities are listed in Table 2. The most remarkable result is the dramatic red shift of the H-bonded OH stretch frequency by nearly 1400 cm^{-1} in SA(H) upon electronic excitation. The OH stretch line thus is located just above the ring-bending vibrations of SA(H). The CO stretch, on the other hand, loses intensity and disappears among the ring-bending vibrations (see Figure 4). In SA(D), the OD line is located at even lower energy (1551 cm^{-1}) and is embedded in a dense manifold of ring vibrations. In both SA(H) and SA(D), the normal mode eigenvector indicates that the OH/OD stretching motion is strongly coupled with deformation and stretching motions of the H-chelate ring.

The present results fully support the conjecture of ref 6 that the H-bonded OH stretch line in the S_1 state of SA is below the detection limit of 2400 cm^{-1} of that experiment. We hope that the present predictions may stimulate a reinvestigation of the S_1 IR spectrum of SA in the frequency range below 2000 cm^{-1}.

5. Conclusions

We have employed the TDDFT/B3LYP method to determine the equilibrium geometry and the vibrational spectrum of AA

and SA in the $S_1(\pi\pi^*)$ state. In both systems, a single minimum of the S_1 potential-energy surface is predicted, which is closer to the amino (enol) form of AA (SA) than to the imino (keto) form. This result confirms previous conjectures for SA.[3−9] The geometry rearrangement after excitation of the S_1 state of AA and SA is better characterized as a H-atom dislocation than a hydrogen-transfer process.

The electronic excitation results, however, in a significant increase of the strength of the intramolecular hydrogen bond. The TDDFT results for SA confirm the existence of an exceptionally strong intramolecular hydrogen bond in the $S_1(\pi\pi^*)$ state. The calculated S_1 equilibrium geometry indicates a pronounced bond conjugation within the H-chelate ring of SA. As a result, the IR spectrum of the S_1 state of SA differs substantially from the S_0 IR spectrum. The calculation predicts a red shift of the phenolic OH stretching vibration by about 1400 cm^{-1}. This dramatic red shift explains why this fingerprint vibration could not be detected in the spectra of ref 6, which had a lower limit of 2400 cm^{-1}.

In AA, the H-chelate ring conjugation in the $S_1(\pi\pi^*)$ state is less pronounced. For the H-bonded amino NH vibration, a red shift of 500 cm^{-1} is calculated in excellent agreement with the recent experiment of Southern et al.[6] This result provides strong support for the reliability of the TDDFT/B3LYP method for the calculation of vibrational spectra of excited states of intramolecularly H-bonded aromatic systems.

Acknowledgment. This work has been supported by the Deutsche Forschungsgemeinschaft and the Committee for Scientific Research of Poland. The authors appreciate the important work of the developers of TURBOMOLE, which has made computational studies like this one possible.

References and Notes

(1) Weller, A. *Prog React. Kinet. Mech.* **1961**, *1*, 187.

(2) Heimbrook, L.; Kenny, J. E.; Kohler, B. E.; Scott, G. W. *J. Phys. Chem.* **1983**, *87*, 280.

(3) Nagaoka, S.; Nagashima, U. *Chem. Phys.* **1989**, *206*, 353.

(4) Bisht, P. B.; Petek, H.; Yoshihara, K.; Nagashima, U. *J. Chem. Phys.* **1995**, *103*, 5290.

(5) Lahmani, F.; Zehnacker-Rentien, A. *J. Phys. Chem.* A **1997**, *101*, 6141.

(6) Yahagi, T.; Fujii, A.; Ebata, T.; Mikami, N. *J. Phys. Chem.* A **2001**, *105*, 10673.

(7) Sobolewski, A. L.; Domcke, W. *Chem. Phys.* **1995**, *184*, 115.

(8) Vener, M. V.; Scheiner, S. *J. Phys. Chem.* **1995**, *99*, 642.

(9) Sobolewski, A. L.; Domcke, W. *Phys. Chem. Chem. Phys.* **1999**, *1*, 3065.

(10) Zwier, T. S. *Annu. Rev. Phys. Chem.* **1996**, *47*, 205.

(11) Mikami, N. *Bull. Chem. Soc. Jpn.* **1995**, *68*, 683.

(12) Southern, D. A.; Levy, D. H.; Florio, G. M.; Longarte, A.; Zwier, T. S. *J. Phys. Chem. A* **2003**, *107*, 4032.

(13) **S**tears, J. A.; Das, A.; Zwier, T. S. *Phys. Chem. Chem. Phys.* **2004**, *6*, 2605.

(14) Sobolewski, A. L.; Domcke, W. *J. Phys. Chem.* A **1999**, *103*, 4494.

(15) Bauernschmitt, R.; Ahlrichs, R. *Chem. Phys. Lett.* **1996**, *256*, 454.

(16) Wiberg, K. B.; Stratman, R. E.; Frisch, M. J. *Chem. Phys. Lett.* **1998**, *297*, 60.

(17) van Caillie, C.; Amos, R. D. *Chem. Phys. Lett.* **2000**, *317*, 159.

(18) Furche, F.; Ahlrichs, R. *J. Chem. Phys.* **2002**, *117*, 7433.

(19) Hutter, J. *J. Chem. Phys.* **2003**, *118*, 3928.

(20) Becke, A. D. *J. Chem. Phys.* **1993**, *98*, 5648.

(21) Woon, D. E.; Dunning, T. H., Jr. *J. Chem. Phys.* **1993**, *98*, 1358.

(22) Ahlrichs, R.; Bär, M.; Häser, M.; Horn, H.; Kölmel, C. *Chem. Phys. Lett.* **1989**, *162*, 165.

(23) A more complete investigation of the topology of the potential-energy surface of the S_1 state of SA shows that it is an extremely flat function of the OH distance. For example, in the range $R_{OH} = 1.0-1.5$ Å, it varies by less than 0.5 kcal/mol.